High Energy Density Physics 7 (2011) 54–60

Contents lists available at ScienceDirect

High Energy Density Physics

journal homepage: www.elsevier.com/locate/hedp

Plasma screening effects on the atomic structure and radiative opacity of dense carbon plasmas based on the DLA model

Cheng Gao, Jiaolong Zeng, Jianmin Yuan*

Department of Physics, College of Science, National University of Defense Technology, Changsha Hunan 410073, PR China

ARTICLE INFO

Article history:
Received 26 January 2011
Accepted 26 January 2011
Available online 4 February 2011

Keywords:
Plasma screening effects
Debye-Hückel model
Radiative opacity

ABSTRACT

A study of plasma screening effects using a Debye-Hückel model is presented. The effects on the energy levels, oscillator strengths, ionization potential and photoionization cross sections of different ionization stages of carbon and on the radiative opacity of hot dense carbon plasmas are presented. The treatment of the atomic structure and radiative opacity is based on the detailed fine-structure level accounting formalism. For the basic atomic data, we compare our calculated energy levels and oscillator strengths with other theoretical results available in the literature and good agreement is found. The calculated ionization potential depressions of helium-like carbon, C V, are compared with the experimental and other theoretical results for a variety of plasma condition. Since the Saha–Boltzmann equation, which determines the ion stage populations, is dependent on the energy levels and ionization potentials of all ionization stages of carbon, the plasma screening effects on these quantities were included to obtain the population distribution. The screening effects play an important role on the spectrally resolved opacity by affecting the position and intensity of the absorption peaks and the K-shell ionization thresholds. With the decrease of Debye screening length, the number and intensity of the absorption peaks are reduced. In particular, the continuum opacity near the K-edge will be so sufficiently affected by the screening effects as to be experimentally observed. Finally, the plasma screening effects on the Rosseland and Planck mean opacities are investigated.

1. Introduction

The experimental and theoretical research of radiative opacity of hot dense plasmas has been of great interest in inertial confinement fusion (ICF) [1], Stellar Physics [2] and X-ray lasers. During past few decades, theoretical models such as unresolved transition arrays (UTA) [3], super transition arrays (STA) [4,5], average atom (AA) [6], detailed term accounting (DTA) [7–10] and detailed level accounting (DLA) models [11] were developed to investigate the radiative opacity of plasmas. In dense plasmas, the interactions of the charged particles are usually screened by the surrounding ions and electrons, resulting in changes of energy levels, electron transition properties and photoionization cross sections when compared with free ions in vacuum. More recently, theoretical work has been carried out to investigate the screening effects on the atomic data such as the energy levels and oscillator strengths by using various models such as Debye-Hückel, ion-sphere and that of a self-consistent potential [12–15]. Most of these works were focused on the few-electron systems such as atomic hydrogen or hydrogen-like ions [16–19] and atomic helium or helium-like ions [20–24]. For multi-electron atoms or ions, there have been relatively fewer efforts [25–29]. There is also some research that deals with the photoionization process [30–35]. For quantum plasmas, an exponential-cosine-screened Coulomb potential was introduced to study the plasma environment effects on the energy levels and oscillator strengths of atoms [36,37].

With the development of experimental technology, denser and denser plasmas near or even above the solid density should be accessible in the laboratory. Therefore, accurate radiative opacities are needed for dense laboratory plasmas, which occur in ICF research and astrophysical research. It indicates that one should include the screening effects caused by the dense plasma environment. As examples of the attempts to introduce the screening effects in a consistent manner we note the following: 1) Crowley [38] developed the CASSANDRA code to calculate the radiative opacity of dense plasmas by introducing the local density approximation (LDA) in an AA model. 2) An improved STA model describes the ionized electrons in the framework of quantum mechanics [39,40]. An optimized effective potential and the LDA approximation are used to calculate the ionization lowering. The shape resonance orbitals just

* Corresponding author.
E-mail address: jmyuan@nudt.edu.cn (J. Yuan).

1574-1818/$ – see front matter © 2011 Elsevier B.V. All rights reserved.
doi:10.1016/j.hedp.2011.01.001

above the ionization threshold are included for the description of the pressure-induced ionization process with the increasing density. 3) In the most recent DLA model, Li et al. [41] carried out a detailed treatment of the plasma environment effects on the atomic structure and radiative opacity of solid dense plasma by introducing a self-consistent potential. Yet their detailed treatment only included the bound–bound opacity, and did not take into account of the plasma screening effects on the bound-free opacity. Thus, there is an obvious need to accurately consider all plasma processes relevant for the calculation of the radiative opacity with the screening effects being taken into account.

This work investigates the screening effects on the radiative opacity of hot dense carbon plasmas by using a DLA model. After introducing the theoretical method of the present work in Section 2, we first show detailed plasma screening effects on the bound–bound and bound-free processes of carbon ions and then the plasma screening on the radiative opacities of carbon plasmas in Section 3. A brief conclusion is given in the last section.

2. Theoretical methods

The details of the DLA model can be found elsewhere [10,11], here we only give a brief outline in the following. For an LTE plasma with temperature T and mass density ρ (or electron density), the radiative opacity at photon energy $h\nu$ is given by

$$\rho\kappa'(h\nu) = \left[\mu_{bb}(h\nu)+\mu_{bf}(h\nu)+\mu_{ff}(h\nu)\right]\left(1-e^{-h\nu/kT}\right)+\mu_{scatt}(h\nu) \tag{1}$$

where μ_{bb}, μ_{bf}, μ_{ff} and μ_{scatt} are the absorption coefficients contributed by the bound–bound, bound-free (photoionization), free–free and scattering processes, respectively and k is the Boltzmann constant.

The bound–bound absorption coefficient μ_{bb} can be expressed as

$$\mu_{bb}(h\nu) = \sum_i\left[\sum_{ll'} N_{il}\sigma_{ill'}(h\nu)\right] \tag{2}$$

where N_{il} is the population of energy level l of ion i and $\sigma_{ill'}$ is the cross section for the photoexcitation from levels l to l' of ion i. For LTE plasmas, N_{il} can be obtained from the Boltzmann distribution function

$$N_{il} = \frac{g_{il}e^{-E_{il}/kT}}{Z_i}N_i \tag{3}$$

where N_i is the total population of ion i, g_{il} is the statistical weight of the level l of ion i, E_{il} is the energy of level l of ionization stage i above the ground level. Z_i is the partition function of ion i, which is obtained by summing over all bound levels of ion i

$$Z_i = \sum_l g_{il}e^{-E_{il}/kT} \tag{4}$$

The populations of the different ionization stages N_i are obtained by solving the Saha-Blotzmann ionization equilibrium equation [42]

$$\frac{N_{i+1}N_e}{N_i} = \frac{Z_eZ_{i+1}}{Z_i}e^{-\phi_i/kT} \tag{5}$$

Due to the influence of plasma environment, the ionization potential ϕ_i is depressed by an amount $\Delta\phi_i$. The consideration of ionization potential depression (IPD) leads to limited number of bound levels for all ionization stages of ions [10]. For a given transition from levels l to l' of ion i, the photoexcitation cross section is given by

$$\sigma_{ill'}(h\nu) = \frac{\pi he^2}{m_ec}f_{ill'}S(h\nu) \tag{6}$$

where $f_{iil'}$ is the oscillator strength for a bound–bound transition from levels l to l' of ion i and $S(h\nu)$ is the line-shape function which is assumed to be a Voigt profile [10]. The line widths contributed by the electron impact broadening [43,44] and Doppler broadening mechanisms [42] were taken into account.

The bound-free absorption coefficient μ_{bf} is contributed from all of the bound levels of all ions

$$\mu_{bf}(h\nu) = \sum_{il} N_{il}\sigma_{il}(h\nu) \tag{7}$$

where $\sigma_{il}(h\nu)$ is the photoionization cross section of energy level l of the ion i.

From the above description, we can see that a large amount of atomic data such as energy levels, oscillator strengths and photo-ionization cross sections are required to calculate the radiative opacity. If the density of the plasma is much smaller than the solid density, the particles can be assumed to be free atoms or ions, then the required atomic data are obtained by solving the Dirac–Fock equation with the Hamiltonian expressed in atomic unit as

$$H = \sum_i\left(c\alpha\cdot p+(\beta-1)c^2-\frac{Z}{r_i}\right)+\frac{1}{2}\sum_{i>j}\frac{1}{r_{ij}} \tag{8}$$

where the terms in the parentheses are the kinetic energy of the ith electron and Coulomb potential with nucleus and the last term represents the Coulomb potential between the electrons. If the plasma density is so high that it is near or above solid density, the plasma environment will modify the Coulomb potential between charged particles. For simplicity, in this work, we consider the screening effects by assuming a Debye-Hückel model with the Coulomb potential being modified to a screened Coulomb potential

$$H' = \sum_i\left(c\alpha\cdot p+(\beta-1)c^2-\frac{Ze^{-r_i/\lambda_D}}{r_i}\right)+\frac{1}{2}\sum_{i>j}\frac{e^{-r_{ij}/\lambda_D}}{r_{ij}} \tag{9}$$

where $\lambda_D = \sqrt{kT_e/4\pi n_e}$ is Debye screening length. The wave-function of bound as well as continuum orbitals are obtained by solving the Dirac–Fock equation represented by the above Hamiltonian and then the oscillator strengths and photoionization cross sections can be calculated. Moreover, the finite number of bound states and IPD are naturally determined by solving the wave equation with Hamiltonian of the form Eq. (9).

3. Results and discussion

3.1. Plasma screening effects on the energy levels and bound–bound transitions

Compared with free ions in vacuum, the plasma screening of charged particles alters the electronic transition properties of ions embedded in plasmas, and therefore influences the opacity of plasmas. Before we discuss the plasma screening effects on the opacity, we first investigate the screening effects on the energy levels and radiative properties of neutral and ionized carbon. Table 1 shows the transition energies and oscillator strengths of C VI for Debye screening lengths: $\lambda_D = \infty$, $10a_0$, $5a_0$, $3.33a_0$ and $2a_0$, where a_0 is Bohr radius and $\lambda_D = \infty$ refers to free ions in vacuum. We chose hydrogen-like C VI ion as an example because there are results in the literature so that we can compare with theoretical results in the literature. For each transition, we give the transition

Table 1
The excitation energy (in eV) and oscillator strength for the bound–bound transitions of C VI at different plasma screening length λ_D. For each transition, the first line gives the excitation energy and the second line the oscillator strength. The last column represents results of NIST [45].

Transitions	λ_D (a_0)					NIST [45]
	∞	10	5	3.33	2	
$1s_{1/2}$–$2p_{1/2}$	367.47	367.01	365.71	363.63	357.39	367.47
	0.2772	0.2761	0.2728	0.2677	0.2522	0.277
$1s_{1/2}$–$2p_{3/2}$	367.53	367.07	365.77	363.69	357.44	367.53
	0.5545	0.5522	0.5456	0.5354	0.5044	0.5542
$1s_{1/2}$–$3p_{1/2}$	435.54	434.16	430.38	424.59	407.94	435.55
	0.0527	0.0515	0.0484	0.0438	0.0299	0.0527
$1s_{1/2}$–$3p_{3/2}$	435.56	434.18	430.40	424.60	407.95	435.56
	0.1055	0.1031	0.0970	0.0877	0.0598	0.1053
$1s_{1/2}$–$4p_{1/2}$	459.36	456.80	450.10	440.23		459.37
	0.0193	0.0179	0.0145	0.0096		0.0193
$1s_{1/2}$–$4p_{3/2}$	459.37	456.81	450.11	440.24		459.38
	0.0386	0.0359	0.0291	0.0193		0.0386
$2s_{1/2}$–$3p_{1/2}$	68.069	67.274	65.150	61.967	53.020	68.07
	0.2899	0.2840	0.2684	0.2443	0.1695	0.2892
$2s_{1/2}$–$3p_{3/2}$	68.087	67.290	65.166	61.981	53.029	68.09
	0.5786	0.5669	0.5356	0.4875	0.3380	0.5786
$1s_{1/2}$–$4p_{1/2}$	91.892	89.912	84.874	77.615		91.893
	0.0685	0.0648	0.0552	0.0392		0.0684
$2s_{1/2}$–$4p_{3/2}$	91.900	89.919	84.879	77.618		91.900
	0.1369	0.1294	0.1102	0.0782		0.1368
$2p_{1/2}$–$3d_{3/2}$	68.090	67.402	65.514	62.583	53.690	68.090
	1.3903	1.3707	1.3159	1.2234	0.8331	1.391
$2p_{3/2}$–$3d_{3/2}$	68.031	67.344	65.457	62.527	53.640	68.031
	0.2782	0.2743	0.2634	0.2449	0.1668	0.278
$2p_{3/2}$–$3d_{5/2}$	68.037	67.350	65.462	62.532	53.642	68.037
	2.5045	2.4692	2.3706	2.2041	1.5008	2.500
$2p_{1/2}$–$4d_{3/2}$	91.903	90.006	85.045	77.608		91.903
	0.2436	0.2343	0.2068	0.1463		0.2436
$2p_{3/2}$–$4d_{3/2}$	91.844	89.947	84.988	77.553		91.844
	0.0487	0.0468	0.0413	0.0293		0.0487
$2p_{3/2}$–$4d_{5/2}$	91.847	89.949	84.990	77.554		91.847
	0.4386	0.4218	0.3722	0.2635		0.438

energy in the first line and oscillator strength in the second line. For comparison, the results from NIST [45] are also given in the last column, which refer to isolated ions and are usually used as a standard.

From the inspection of Table 1, one can see that our theoretical results for $\lambda_D = \infty$ agrees excellently with those of NIST [45]. It should be noted that both the transition energy and oscillator strength decrease for a given transition with the decrease of Debye screening length; however, the degree of variation is distinct for different transitions. Except for the transitions of $1s$–$2p$ ($1s_{1/2}$–$2p_{1/2}$ and $1s_{1/2}$–$2p_{3/2}$), the excitation energy of other transitions decrease evidently with the decrease of λ_D. For example, the excitation energies of $1s_{1/2}$–$2p_{1/2}$, $1s_{1/2}$–$3p_{1/2}$ and $1s_{1/2}$–$4p_{1/2}$ at $\lambda_D = 3.33a_0$ decrease by 1.04%, 2.51% and 4.16%, respectively, compared with that at $\lambda_D = \infty$. Since λ_D is proportional to the ratio $(T/n_e)^{1/2}$, this means that the transition energy becomes more and more redshifted as the plasma density increases for a given plasma temperature. Such a variational trend is a reflection of the IPD, which can be seen from Table 2. As the IPD of $1s_{1/2}$, $2p_{1/2}$, and $2p_{3/2}$ orbitals vary slowly with λ_D, resulting in the smaller changes of the excitation energy of $1s$–$2p$ transitions than higher principle quantum number levels. From the inspection of Table 2, one can see that the IPD of the electronic orbitals is basically determined by the principal quantum number of the orbitals. The ionization potential is only 1.55 eV for $4d$ electron at $\lambda_D = 3.33a_0$, while $4f$ electron is merged into the continuum. With the further decrease of Debye screening length up to $\lambda_D = 2a_0$, $4d$, $4p$ and $4s$ orbitals become continuum orbitals and only orbitals with principal quantum number less than 4 (i.e., $1s_{1/2}$, $2s_{1/2}$, $2p_{1/2}$, $2p_{3/2}$, $3s_{1/2}$, $3p_{1/2}$, $3p_{3/2}$, $3d_{3/2}$ and $3p_{5/2}$) are bound. The oscillator strength varies in the same manner as the excitation energy, that is, it decreases with the decrease of λ_D. Taking the transitions of $1s_{1/2}$–$np_{1/2}$, (n = 2,3,4), we found that the oscillator strength decreases by 3.43%, 16.73% and 50.26%, respectively, for $\lambda_D = 3.33a_0$. For $\lambda_D = 2a_0$, the orbitals with the principal quantum number higher than 3 have merged into continuum and therefore the excitation energies and oscillator strengths for transitions of $1s$–$4p$, $2s$–$4p$ and $2p$–$4d$ are absent in Table 1.

Most studies of the plasma screening effects on the oscillator strengths published in the literature were carried out in the framework of the non-relativistic atomic theory by using a Debye-Hückel potential. To have a quantitative comparison with the

Table 2
The ionization potential (in eV) of different relativistic electron orbitals of C VI at different plasma screening length λ_D.

Orbitals	λ_D (a_0)				
	∞	10	5	3.33	2
$1s_{1/2}$	489.99	473.87	458.14	442.79	413.25
$2s_{1/2}$	122.52	106.97	92.90	80.16	58.29
$2p_{1/2}$	122.52	106.85	92.43	79.16	55.82
$2p_{3/2}$	122.46	106.79	92.37	79.10	55.77
$3s_{1/2}$	54.45	39.82	28.16	18.98	6.73
$3p_{1/2}$	54.45	39.70	27.75	18.20	5.26
$3p_{3/2}$	54.43	39.68	27.74	18.18	5.25
$3d_{3/2}$	54.43	39.45	26.91	16.57	2.13
$3d_{5/2}$	54.42	39.44	26.91	16.57	2.12
$4s_{1/2}$	30.62	17.17	8.34	3.03	
$4p_{1/2}$	30.62	17.06	8.03	2.55	
$4p_{3/2}$	30.62	17.06	8.02	2.55	
$4d_{3/2}$	30.62	16.85	7.38	1.55	
$4d_{5/2}$	30.61	16.85	7.38	1.55	
$4f_{5/2}$	30.61	16.52	6.38		
$4f_{7/2}$	30.61	16.52	6.38		

Table 3
Comparison of oscillator strengths of transitions $1s-np$ (n = 2, 3, 4, 5) of C VI at a variety of plasma screening length λ_D with available work [16,46,47], which are remarked by superscript a, b and c, respectively.

λ_D (a_0)	$1s-2p$	$1s-3p$	$1s-4p$	$1s-5p$
∞	0.4159	0.0791	0.0290	0.0139
	0.4162[a]	0.0791[a]	0.0290[a]	0.0139[a]
16.67	0.4152	0.0784	0.0281	0.0130
	0.4155[a]	0.0785[a]	0.02812[a]	0.0130[a]
	0.416[b]	0.0784[b]	0.0282[b]	0.0130[b]
8.33	0.4134	0.0766	0.0261	0.0107
	0.4136[a]	0.0767[a]	0.0261[a]	0.0108[a]
	0.410[b]	0.0728[b]	0.0219[b]	0.00635[b]
6.67	0.4120	0.0753	0.0247	0.0092
	0.4123[a]	0.0754[a]	0.0247[a]	0.00926[a]
3.33	0.4015	0.0658	0.0145	
	0.40175[a]	0.06585[a]	0.01448[a]	
	0.402[b]	0.0658[b]	0.0145[b]	
	0.40165[c]	0.06579[c]	0.01448[c]	
1.67	0.3628	0.0298		
	0.3630[a]	0.0298[a]		
0.83	0.1933			
	0.1933[a]			

available work, we give the oscillator strengths of the non-relativistic results for Lyman and Balmer series of C VI at a variety of λ_D from this work and other theoretical results [16,46,47] in Tables 3 and 4, respectively. The non-relativistic results reported in this work are obtained from relativistic calculations, that is, by summing over the final states and averaging over the initial states for all transitions of a particular transition array

$$f\left(n_i l_i - n_f l_f\right) = \frac{\sum_k (2j_k+1) \sum_m f\left(n_i l_i j_k - n_f l_f j_m\right)}{\sum_k (2j_k+1)} \quad (10)$$

where $f(n_i l_i j_k - n_f l_f j_m)$ is the relativistic oscillator strength obtained by solving the wave equation with Hamiltonian represented by Eq. (9), $f(n_i l_i - n_f l_f)$is corresponding non-relativistic result and $(2j_k + 1)$ is the statistical weight of the initial bound level. It can be seen that excellent agreement is found between different theoretical results for the values of λ_D.

3.2. Plasma screening effects on the photoionization cross sections

As shown in the above, the ionization potential of electronic orbitals can be dramatically reduced by the plasma screening effects. With the change of ionization potential, the photoionization cross sections for a particular level will surely be altered.

Table 4
Comparison of oscillator strengths of Balmer series of C VI for a variety of plasma screening length λ_D with work carried out by Qi et al. [16], which are remarked by superscript *a*.

λ_D (a_0)	$2s-3p$	$2s-4p$	$2s-5p$	$2s-3d$	$2s-4d$	$2s-5d$
∞	0.4343	0.1027	0.0419	0.6955	0.1218	0.0444
	0.435[a]	0.103[a]	0.0419[a]	0.696[a]	0.122[a]	0.0444[a]
16.67	0.4309	0.1005	0.0396	0.6918	0.1200	0.0424
	0.431[a]	0.101[a]	0.0396[a]	0.692[a]	0.120[a]	0.0424[a]
8.33	0.4218	0.0949	0.0340	0.6816	0.1152	0.0372
	0.422[a]	0.095[a]	0.0340[a]	0.682[a]	0.115[a]	0.0372[a]
6.67	0.4154	0.0910	0.0300	0.6742	0.1116	0.0332
	0.416[a]	0.091[a]	0.03[a]	0.674[a]	0.112[a]	0.0332[a]
3.33	0.3659	0.0587		0.6162	0.0732	
	0.367[a]	0.0587[a]		0.612[a]		
1.67	0.1709					
	0.171[a]					

Maksimchuk et al. [48] measured the IPD of helium-like C V at a variety of temperature and electron density of hot dense plasmas by an intense ultrashort laser pulse. The temperature and electron density of the carbon plasma were deduced from the simulation of experimental spectra at a few time points after the start of emission of carbon target. At the measured time of 0, 20, 30 and 40 ps, the plasma temperature is diagnosed to be 71, 76, 78 and 76 eV, and the electron density to be 5.0×, 3.0×, 1.5× and 0.8 × 10^{22} cm^{-3}, respectively. Fig. 1 shows the IPD of C V in the environment of the above plasma condition. For comparison, the experimental measurement and a number of theoretical calculations carried out by Maksimchuk et al. [48] and by Gil et al. [49] are shown in this figure. Among these theoretical calculations, the results obtained by the Stewart-Pyatt (SP) model of Gil et al. [49], the nonisolated analytical potential (NIP) model and the SP model of Maksimchuk et al. [48] agree best with the experiment. The SP model combines both Debye and ion-sphere models, thus it should be better than Debye or ion-sphere model in describing the IPD for the plasma condition in the experiment carried out by Maksimchuk et al. [48]. However, we do not know how these authors applied these models to obtain their results as there was little detailed description in their original work [49,48]. Thus it is not clear for the physical origin of the difference between the results of two SP models of Gil et al. [49] and Maksimchuk et al. [48]. The Debye model used in this work and ion-sphere model of Gil et al. [49] predicted the same trends with the experiment for the IPD, although our calculated IPD is smaller than the experiment while Gil et al. [49] predicted slightly larger values. How to find the most suitable potential to describe the plasma screening effects at different density region and how to apply them await further investigation.

The change of ionization potential means the shift of ionization threshold of the energy levels and therefore alters the ionization cross sections. The plasma screening effects on the photoionization process can be seen from Fig. 2, which shows the photoionization cross sections of the ground level $1s^2\,{}^1S_{1/2}$ of C V ion. The ionization

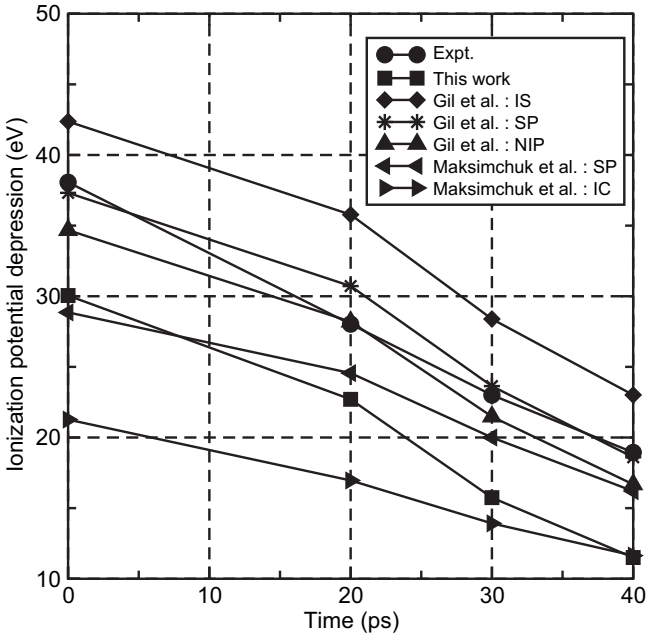

Fig. 1. The IPD of C V at a variety of plasma condition. A number of theoretical results are given, including the ion-sphere (IS) (diamond), Stewart-Pyatt (SP) (star) and nonisolated analytical potential (NIP) (up triangle) models carried out by Gil et al. [49] and the SP (left triangle) and ion-cell (IC) (right triangle) models by Maksimchuk et al. [48].

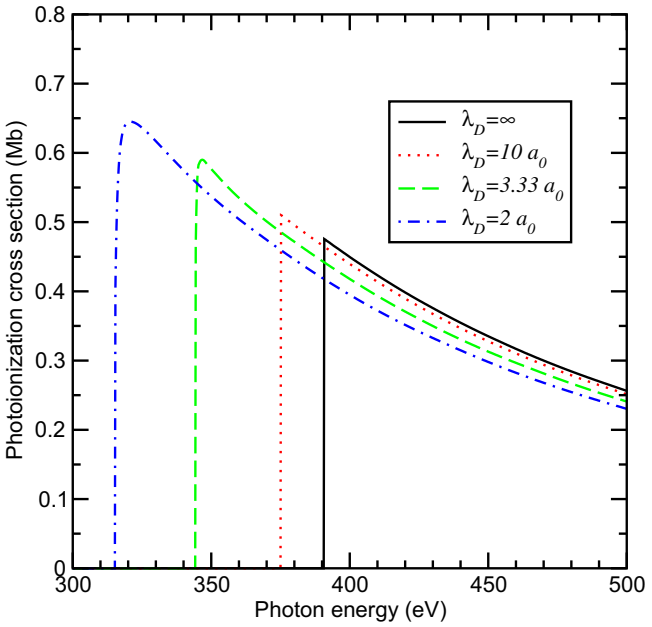

Fig. 2. The photoionization cross section of energy level $1s^2_{1/2}{}^1S_0$ of C V as a function of photon energy at Debye screening length $\lambda_D = \infty$, $10a_0$, $3.33a_0$ and $2a_0$.

potential decreases with the decrease of screening length λ_D, resulting in the increase of photoionization cross sections near their respective thresholds. However, above the ionization threshold of the free ion, the screening effects tend to reduce the photoionization cross section. This means that the screening of free electrons reduces the direct ionization cross section if the screening effects on the bound levels are neglected. In fact, one needs to take both the screening effects on the free electrons and on the bound levels into account. As a result, the sum rule for the total oscillator strengths is automatically conserved. Unfortunately, there is little work reported for the plasma screening effects on the photoionization cross sections for carbon ions.

3.3. *Plasma screening effects on the radiative opacity of carbon plasmas*

To calculate the radiative opacity of plasmas in LTE, one has to determine the populations of the different charge states. To obtain this, one needs the partition function and ionization potential of all ionization stages to solve the Saha–Boltzmann equation (5). If we do not consider the effects of the plasma environment, the partition function is divergent because of the infinite number of atomic states for free atoms or ions with the Hamiltonian of Eq. (8). However, the screened Coulomb potential can support only a finite number of bound states, which implies that the binding energy of bound states decreases with decreasing of λ_D. In principle, the finite number of bound states and the IPD should be determined by solving the wave equation with the Hamiltonian represented by Eq. (9). In practice, a number of simplified methods [50,12], such as the Debye-Hückel, Stewart-Pyatt and ion-sphere models, were developed to calculate the IPD and therefore to determine the finite number of bound states. For the Debye-Hückel model, the depressed amount $\Delta\phi_i$ (Eq. (5)) is expressed in atomic unit as

$$\Delta\phi_i = z\sqrt{\frac{4\pi n_e}{kT}} \tag{11}$$

where z is the effective nuclear charge number of ion i. For low density plasmas the effects of the plasma environment are commonly taken into account by such a method, which is widely used in detailed and statistic models for the calculation of radiative opacities. For the generation of radiative opacity it is difficult to introduce the effects of the plasma environment on the atomic data by using such a method, because in denser plasmas, such effects are sufficiently pronounced that one must take these effects into account self-consistently. From Eqs. (6) and (7), these atomic data include the oscillator strengths and photoionization cross sections. The effects of the plasma environment on these atomic data can be found by solving the wave equation with a modified screened Coulomb potential (Eq. (9)) for the Debye-Hückel model. However, in practice, it is difficult to do this from Eq. (11). On the other hand, by solving the Dirac–Fock equation for the electrons with the Hamiltonian represented in Eq. (9), one can self-consistently determine the Debye screening effects on the radiative opacity. In this way, the Debye screening effects on both the charge state populations and on the atomic data can be taken into account.

Fig. 3 shows the spectrally resolved radiative opacity (mass absorption coefficient) of carbon plasmas at a temperature of 100 eV for a selected screening length at (a) $\lambda_D = 10a_0$ (corresponding to electron density of 2.0×10^{22} cm^{-3}), (b) $\lambda_D = 3.33a_0$ (electron density of 1.77×10^{23} cm^{-3}) and (c) $\lambda_D = 2a_0$ (electron density of 4.95×10^{23} cm^{-3}), respectively, obtained by using the two methods described above. In the first, Debye screening was used to truncate the bound states to get a convergent partition function and IPD to solve the Saha–Boltzmann equation. It is implemented by considering an IPD $\Delta\phi_i$ given by Eq. (11). The transition energies, oscillator strengths and photoionization cross sections required in the calculation of opacity are obtained by solving the Dirac–Fock equation with the Hamiltonian represented by Eq. (8) for free atoms or ions. This is the common practice that was widely used in different models such as DLA [11]. The results are shown in Fig. 3 by dashed lines. For the second set of results, we took into account of the plasma screening effects on all atomic data including energy levels, oscillator strengths and photoionization cross sections required in the calculation of opacity and therefore the screening effects on the opacity were fully included. The population distributions of the different charge states were obtained by

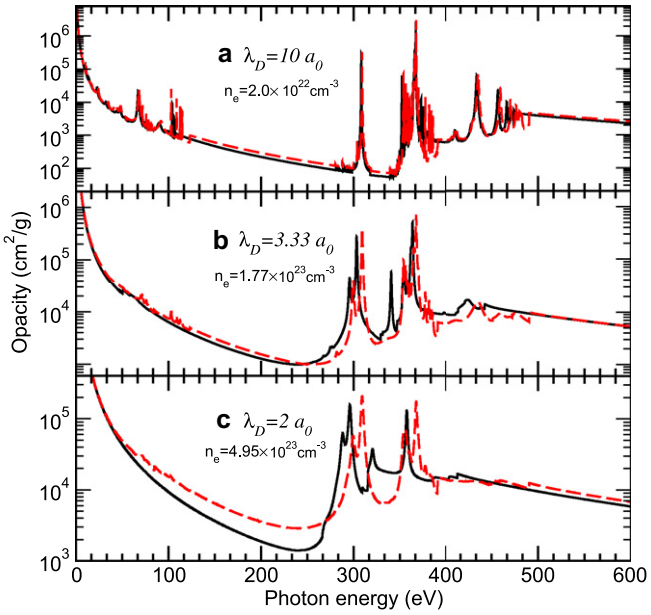

Fig. 3. Spectrally resolved radiative opacity (mass absorption coefficient) of carbon plasmas at the temperature of 100 eV and Debye screening length λ_D of (a) $10a_0$, (b) $3.33a_0$ and (c) $2a_0$. The solid and dashed lines represent results with and without considering screening effects.

solving the Saha–Boltzmann equation with the plasma screening effects being included in the ionization potentials and the partition functions, which is also determined by solving the wave equation with Hamiltonian represented by Eq. (9). The results were shown in Fig. 3 in solid lines.

At the screening length $\lambda_D = 10a_0$, we can see that there are two major absorption structures located at 0–120 eV and 280–500 eV for both methods. The absorption structures located at region of 0–120 eV originate from the transitions from the excited levels of carbon ions with the principal quantum number of the electron orbitals ≥2. The absorption peaks near 300 and 380 eV originate from the $1s \rightarrow 2p$ transitions of C V and C VI, respectively, while other peaks at higher photon energy arise from $1s \rightarrow np\,(n \geq 3)$ transitions of C VI.

The plasma screening effects on the radiative opacity can clearly be seen from Fig. 3a–c with the decrease of λ_D. Firstly, the screening effects tend to lower the transition energy and reduce the absorption intensity of the absorption peaks, yet they behave differently. For the transition energy, the smaller the screening length λ_D, the smaller the transition energy. However, the absorption does not decrease linearly with the decrease of λ_D. For the given three values of λ_D, the absorption decreases most at $\lambda_D = 3.33a_0$. Therefore, one surmises that there exists a plasma condition for which the effects of screening are maximized. For the oscillator strengths, as discussed in the above, decrease monotonically with λ_D. The different trends shown in the opacity and oscillator strengths are due to following factors. First, the absorption peaks are dependent on both the oscillator strengths and populations of relevant quantum states. Secondly, with the decrease of the screening length λ_D, some absorption features begin to disappear from the lowest and the highest photon energy. These structures are caused by transitions from the electron orbitals of higher principal quantum number. Because of the screening effects, these bound electron orbitals with higher principal quantum number are gradually merged into the continuum region. Thirdly, the screening effects affect not only the bound–bound transitions but also the bound-free process. Similar conclusions concerning line position and intensity can be made for the continuum opacity, which can be seen from Fig. 3 in regions of 100–280 and 380–500 eV. Of particular interest is the opacity near the K-edge, which is shown for the bound-free opacity in Fig. 4.

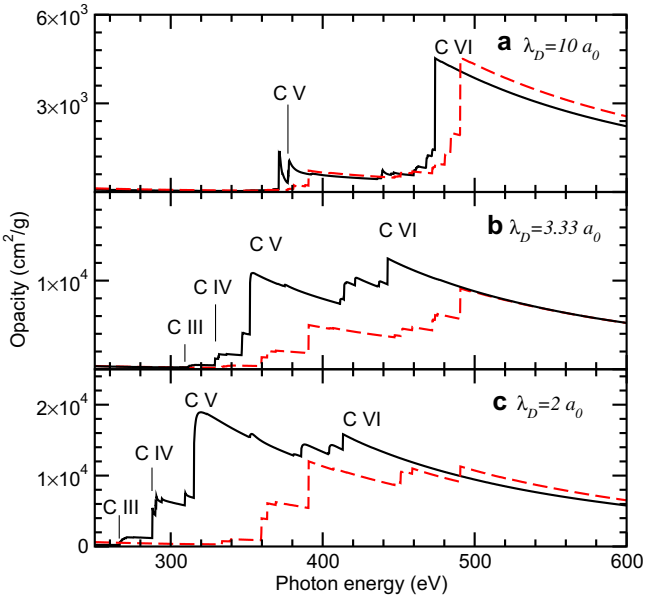

Fig. 4. The bound-free opacity near the K-edge absorption threshold with the same plasma conditions in Fig. 3. The meaning of solid and dashed lines is the same as in Fig. 3. Note that the logarithmic expression was changed to linear for the opacities to show more clearly the screening effect.

Table 5
The Rosseland and Planck mean opacity (in cm²/g) of carbon plasmas at the temperature of 100 eV for a variety of screening length λ_D with and without the screening effects being included.

λ_D (a_0)	Rosseland			Planck		
	With	Without	Rel. diff. (%)	With	Without	Rel. diff. (%)
10	323	397	22.91	3276	3519	7.42
5	1680	2020	20.24	7160	7166	0.08
3.33	3493	3302	−5.47	9658	10,156	5.16
2.5	3962	4934	24.53	11,324	11,738	3.66
2	4813	6181	27.94	12,117	13,467	11.14

From the inspection of Fig. 4, one can see that the plasma screening shows pronounced effects near the K-edge of ionization stages of C III–C VI, especially at $\lambda_D = 3.33a_0$ and $\lambda_D = 2a_0$. The ionization thresholds of the respective ions with the screening effect being included are indicated in the figure. Note that the position of ionization thresholds shown in Figs. 3 and 4 in dashed lines does not change with screening length λ_D as these results were obtained by using the ionization potential of free ions. The opacity near the K-edge of C V and C VI was greatly changed by the plasma screening effect. The pronounced screening effects on the opacity near the K-edge may be a subject for future experimental investigation. As we know, it is not easy to experimentally investigate the screening effects on the energy levels and oscillator strengths of ions. Yet it should be easier to measure the radiative opacity near the K-edge for dense plasmas and therefore to determine the ionization thresholds of the respective ions, which can clearly be seen from Fig. 4. We hope that the present work will be helpful for future experimental design to study the screening effects on the radiative opacity as well as on the atomic structure.

From the above discussion, we can see that Debye screening has strong effects on the spectrally resolved radiative opacity and therefore the mean opacities will be affected. Table 5 shows the Rosseland and Planck mean opacities at a variety of λ_D for carbon plasmas with the temperature being fixed to be 100 eV. With the decrease of λ_D (i.e. the plasma density increases), both Rosseland and Planck mean opacities increase. The agreement between the Planck mean opacities obtained with and without the screening effects is better than those of the Rosseland mean opacities. The relative difference between the Planck mean opacities with and without screening effects is less than 12% for given λ_D values. For Rosseland mean opacity, the largest relative difference amounts to 27%. It should be noted that the coupling parameter Γ [51] is around one for carbon plasma at these conditions, which means the correlation effects between particles should be considered. In this paper, the correlation effects are not taken into account yet. Further work on the correlation effects between the ions and electrons is needed, which is underway.

4. Conclusion

In conclusion, we investigated the Debye screening effects on the atomic structure and radiative opacity of hot dense carbon plasmas over a wide range of Debye screening length λ_D by using the DLA model. The atomic data including the energy levels, oscillator strengths, ionization potentials and photoionization cross sections are calculated over a wide range of plasma density up to the solid-state density with the screening effects being taken into account for all ionization stages of carbon ions from the neutral atom to hydrogen-like ion. Illustrative results are given for hydrogen-like C VI and helium-like C V ions, which are compared with other theoretical and experimental results available in the literature. The screening effects are also investigated in the calculation of the population distribution of different charge states when

solving the Saha–Boltzmann ionization equilibrium equation. The plasma screening effects play an important role on the spectrally resolved opacity by affecting the positions and intensities of the absorption peaks and the positions of the K-shell ionization thresholds. The continuum opacity near the K-edge of C V and C VI is greatly changed with the decrease of Debye screening length. This physical effect shows such pronounced influence on the opacity near the K-edge of C V and C VI that it may be a subject to be experimentally studied. It has great physical implications because the information of the screening effects on the atomic structure can be deduced from the opacity near the K-edge. The present work should be helpful for future experimental design to study the screening effects on the radiative opacity as well as on the atomic structure. The plasma screening effects on the Rosseland and Planck mean opacities are discussed in the last section.

Acknowledgments

This work was supported by the National Natural Science Foundation of China under Grants Nos. 10774191, 10878024 and 10734140, and the National Basic Research Program of China (973 Program) under Grant No. 2007CB815105.

References

[1] E. Storm, Fusion J. Energy 7 (1988) 131.
[2] F.J. Rogers, C.A. Iglesias, Science 263 (1994) 50.
[3] C. Bauche-Arnoult, J. Bauche, M. Klapisch, Phys. Rev. A 20 (1979) 2424 25 (1982) 2641; 30 (1984) 3026; 31 (1985) 2248.
[4] K. Eidmann, A. Bar-Shalom, A. Saemann, G. Winhart, Europhys. Lett. 44 (1998) 459.
[5] A. Bar-Shalom, J. Oreg, W.H. Goldstein, D. Shvarts, A. Zigler, Phys. Rev. A 40 (1989) 3183.
[6] J.M. Yuan, Phys. Rev. E 66 (2002) 047401.
[7] Joseph Abdallah Jr., Robert E.H. Clark, J. Appl. Phys. 69 (1991) 23.
[8] C.A. Iglesias, M.H. Chen, V. Sonnad, B.G. Wilson, J. Quant. Spectrosc. Radiat. Transf. 81 (2003) 227.
[9] Jiaolong Zeng, Fengtao Jin, Jianmin Yuan, Qisheng Lu, Yongsheng Sun, Phys. Rev. E 62 (2000) 7251.
[10] Jiaolong Zeng, Jianmin Yuan, Qisheng Lu, Phys. Rev. E 64 (2001) 066412.
[11] Jiaolong Zeng, Jianmin Yuan, Phys. Rev. E 74 (2006) 025401(R).
[12] P. Debye, E. Hückel, Z. Phys. 24 (1923) 185.
[13] D. Salzmann, H. Szichman, Phys. Rev. A 35 (1987) 807.
[14] B. Saha, S. Fritzsche, J. Phys. B: At. Mol. Opt. Phys. 40 (2007) 259.
[15] Yongqiang Li, Jianhua Wu, Yong Hou, J. Jianmin Yuan, Phys. B: At. Mol. Opt. Phys. 41 (2008) 145002.
[16] Y.Y. Qi, J.G. Wang, R.K. Janev, Phys. Rev. A 78 (2008) 062511.
[17] Gerald J. Iafrate, Lawrence B. Mendelsohn, Phys. Rev. 182 (1969) 244.
[18] J. Seidel, S. Arndt, W.D. Kraeft, Phys. Rev. E 52 (1995) 5387.
[19] S. Paul, Y.K. Ho, Phys. Plasmas 15 (2008) 073301.
[20] J.M. Ugalde, C. Sarasola, X. Lopez, Phys. Rev. A 56 (1997) 1642.
[21] Song-Tao Dai, Alina Solovyova, Peter Winkler, Phys. Rev. E 64 (2001) 016408.
[22] D. Ray, P.K. Mukherjee, J. Phys. B: At. Mol. Opt. Phys. 31 (1998) 3479.
[23] S. Kar, Y.K. Ho, Phys. Rev. E 70 (2004) 066411.
[24] P. Winkler, Phys. Rev. E 53 (1996) 5517.
[25] J.M. Gil, P. Martel, E. Mínguez, J.G. Rubiano, R. Rodríguez, F.H. Ruano, J. Quant. Spectrosc. Radiat. Transf. 75 (2002) 539.
[26] Inaki Silanes, Jose M. Mercero, Jesus M. Ugalde, Phys. Rev. E 66 (2002) 026408.
[27] B. Saha, S. Fritzsche, Phys. Rev. E 73 (2006) 036405.
[28] Yongqiang Li, Jianhua Wu, Jianmin Yuan, Acta Phys. Sin. 57 (2008) 4042 [in Chinese].
[29] S. Paul, Y.K. Ho, Phys. Rev. A 78 (2008) 042711.
[30] Sabyasachi Kar, Y.K. Ho, Phys. Rev. A 77 (2008) 022713.
[31] Y.Y. Qi, Y. Wu, J.G. Wang, Phys. Plasmas 16 (2009) 033507.
[32] Sabyasachi Kar, Y.K. Ho, Phys. Plasmas 13 (2006) 063301.
[33] L.B. Zhao, Y.K. Ho, Phys. Plasmas 11 (2004) 1695.
[34] Young-Dae Jung, Phys. Plasmas 5 (1998) 3781.
[35] Young-Dae Jung, Phys. Plasmas 8 (2001) 3111.
[36] Arijit Ghoshal, Y.K. Ho, J. Phys. B: At. Mol. Opt. Phys. 42 (2009) 075002.
[37] Arijit Ghoshal, Y.K. Ho, Phys. Rev. A 79 (2009) 062514.
[38] B.J.B. Crowley, Phys. Rev. A 41 (1990) 2179;
B.J.B. Crowley, J.W. Harris, J. Quant. Spectrosc. Radiat. Transf. 71 (2001) 257.
[39] A. Bar-Shalom, J. Oreg, M. Klapisch, J. Quant. Spectrosc. Radiat. Transf. 99 (2006) 35;
A. Bar-Shalom, J. Oreg, High Energy Density Phys. 3 (2007) 12.
[40] J.C. Pain, G. Dejonghe, T. Blenski, J. Quant. Spectrosc. Radiat. Transf. 99 (2006) 451.
[41] Yongqiang Li, Jianhua Wu, Yong Hou, J. Jianmin Yuan, Phys. B: At. Mol. Opt. Phys. 42 (2009) 235701.
[42] R.D. Cowan, Theory of Atomic Spectra. University of California Press, Berkeley, 1981.
[43] M.S. Dimitrijevic, N. Konjevic, J. Quant. Spectrosc. Radiat. Transf. 24 (1980) 451.
[44] M.S. Dimitrijevic, N. Konjevic, Astron. Astrophys. 172 (1987) 345.
[45] See NIST Atomic Spectra Data Base. http://physics.nist.gov/cgi-bin/atdata/main-asd.
[46] J.C. Weisheit, B.W. Shore, Astrophys. J. 194 (1974) 519.
[47] F.E. Höhne, R. Zimmermann, J. Phys. B: At. Mol. Opt. Phys. 15 (1982) 2551.
[48] A. Maksimchuk, M. Nantel, G. Ma, S. Gu, C.Y. Côté, D. Umstadter, et al., J. Quant. Spectrosc. Radiat. Transf. 65 (2000) 367.
[49] J.M. Gil, R. Rodríguez, R. Florido, J.G. Rubiano, P. Martel, E. Mínguez, Laser Part. Beams 26 (2008) 21.
[50] G.J. Heading, J.S. Wark, G.R. Bennett, R.W. Lee, J. Quant. Spectrosc. Radiat. Transf. 54 (1995) 167 and references therein.
[51] S. Ichimaru, Rev. Mod. Phys. 54 (1982) 1017.